Composite Structures 267 (2021) 113887

Contents lists available at ScienceDirect

Composite Structures

journal homepage: www.elsevier.com/locate/compstruct

High-precision computation in mechanics of composite structures by a strong sampling surfaces formulation: Application to angle-ply laminates with arbitrary boundary conditions

G.M. Kulikov [a,*], M.G. Kulikov [b]

[a] Laboratory of Intelligent Materials and Structures, Tambov State Technical University, Sovetskaya, 106, Tambov 392000, Russia
[b] Department of Applied Mathematics, Tambov State Technical University, Sovetskaya, 106, Tambov 392000, Russia

ARTICLE INFO

Keywords:
Laminated composite plate
3D stress analysis
Plates with clamped and free edges
Strong SaS formulation
Extended DQ method

ABSTRACT

This paper presents the three-dimensional analysis of laminated composite rectangular plates with general boundary and loading conditions using the strong sampling surfaces (SaS) formulation and the extended differential quadrature (EDQ) method proposed by the first author. The strong SaS formulation is based on the choice of SaS parallel to the middle surface and located at Chebyshev polynomial nodes to introduce the displacements of these surfaces as plate unknowns. This choice of unknowns with the use of Lagrange polynomials in the through-thickness approximations of displacements, strains and stresses leads to an efficient laminated plate formulation. The outer surfaces and interfaces are not included into a set of SaS that makes it possible to minimize uniformly the error due to Lagrange interpolation. Therefore, the strong SaS formulation based on direct integration of the equilibrium equations of elasticity in the transverse direction in conjunction with the EDQ method can be applied effectively to high-precision calculations for the composite rectangular plates with different boundary conditions. This due to the fact that in the SaS/EDQ formulation the displacements, strains and stresses of SaS are interpolated in a rectangular domain using the Chebyshev-Gauss-Lobatto grid and Lagrange polynomials are also utilized as basis functions. Such a technique allows the use of only first order derivatives in the equilibrium equations that simplifies the implementation of the EDQ method.

1. Introduction

Three-dimensional exact solutions for composite plates are of great importance, since the validity of approximate plate theories and plate finite elements can be assessed by comparing their predictions with exact results. In the literature, there are at least five approaches to exact solutions for plates, namely, the displacement-based approach [1,2], the state space approach [3], the power series expansion approach (Frobenius method) [4], the asymptotic approach [5] and the sampling surfaces (SaS) approach [6]. The closed-form solutions for simply supported rectangular plates using the displacement-based approach were obtained in contributions [7–13]. The most popular state space approach was implemented for the bending and vibration analysis of simply supported plates in many papers (see, e.g. [14–17]). The Frobenius method was applied efficiently to analytical solutions for functionally graded rectangular plates by Vel and Batra [18–20]. The exact solutions based on the asymptotic approach for simply supported laminated anisotropic and functionally graded plates were obtained in papers [21–25]. Recently, the SaS approach has been utilized to exact solutions for static and dynamic problems for laminated composite plates and cylindrical panels with simply supported edges [26–29].

As for rectangular plates with different boundary conditions, there is a very limited number of articles devoted to the three-dimensional static and dynamic analysis. The analytical solutions for rectangular plates with free and clamped edges using the displacement-based approach were obtained in [30,31]. The three-dimensional analysis of Levy-type laminated rectangular plates is presented in papers [32,33]. The state space approach was used to evaluate the three-dimensional dynamic response of a clamped laminated plate [34]. The benchmark solutions for isotropic and composite rectangular plates with different boundary conditions using the Ritz method were found in [35–38]. The SaS approach was applied to the three-dimensional vibration analysis of laminated composite plates with free, clamped and simply supported edges [39,40].

The SaS formulation with three SaS has been proposed by the first author [41] and extended to shells with an arbitrary number of equally

* Corresponding author.
E-mail address: gmkulikov@mail.ru (G.M. Kulikov).

https://doi.org/10.1016/j.compstruct.2021.113887
Received 14 March 2021; Accepted 17 March 2021
Available online 23 March 2021

spaced SaS by Kulikov and Plotnikova [42]. The variational formulation with SaS located at the Chebyshev polynomial nodes was developed later [43–45], since the SaS formulation with equispaced SaS does not work properly with the higher order Lagrange interpolation. The use of only Chebyshev polynomial nodes significantly improves the behavior of higher order Lagrange polynomials because such choice makes it possible to minimize uniformly the error caused by Lagrange interpolation [26,46]. This fact allows us to obtain the displacements and stresses with a prescribed accuracy using a sufficient number of SaS. In other words, SaS-based solutions asymptotically approach three-dimensional exact solutions of elasticity if the number of SaS tends to infinity. Note that the implementation of the SaS variational formulation for laminated plates [6,44,45] is impossible without the use of interfaces. On the contrary, the strong SaS formulation [26–29] based on the direct integration of the equilibrium equations of elasticity and the satisfaction of the continuity conditions at the interfaces is free of this restriction. Therefore, the use of interfaces is avoided that allows one to get all the benefits of the higher order Lagrange interpolation with Chebyshev polynomial nodes.

The present paper focuses on the implementation of the strong SaS formulation for the three-dimensional analysis of laminated rectangular plates with free and clamped edges. To solve this problem, the differential quadrature (DQ) method can be used. The DQ method is a numerical technique developed by Bellman and his co-authors [47,48] for solving the boundary value problem for partial differential equations. The original DQ method was applied to problems in structural mechanics by Bert and his co-authors [49,50]. The shortcoming of the DQ method is that the weighting coefficients depend on the grid points and the order of the derivatives in the differential equations. To overcome this shortcoming, Shu and Richards [51] developed the generalized differential quadrature (GDQ) method by introducing recursive relationships for calculating higher order derivatives. The advantage of the GDQ method is that the weighting coefficients are no longer dependent on the grid points and the order of the derivatives when Lagrange polynomials are utilized as basis functions [52]. The GDQ method has been effectively applied to three-dimensional bending, buckling and vibration problems for isotropic and orthotropic rectangular plates with different boundary conditions [53–55]. A historical overview of the DQ and GDQ methods can be found in papers [56,57].

To improve the computational efficiency of the GDQ method, the extended differential quadrature (EDQ) method [58] is employed. A feature of the EDQ method is that not only displacements are interpolated in a rectangular domain using the Chebyshev-Gauss-Lobatto grid and Lagrange polynomials as basis functions. The same technique is applied to the strains and stresses, which are also interpolated by using the Chebyshev-Gauss-Lobatto grid and Lagrange polynomials as basis functions. This, in turn, leads to the use of only first order derivatives in the equilibrium equations (second order derivatives are not required) that greatly simplifies the implementation of the EDQ method. Thus, the strong SaS formulation can be effectively applied to high-precision calculations of laminated composite plates with general boundary and loading conditions.

2. Three-dimensional formulation for laminated rectangular plate

Consider a composite rectangular plate of the thickness h consisting of N elastic layers of the thickness h_n, where $n = 1, 2, \ldots, N$. Let the middle surface Ω be described by Cartesian coordinates x and y, whereas the coordinate z is oriented in the thickness direction (see Fig. 1). Due to the choice of coordinates, the strains of the nth layer $\varepsilon_{ij}^{(n)}$ are expressed as

$$\begin{aligned} 2\varepsilon_{\alpha\beta}^{(n)} &= u_{\alpha,\beta}^{(n)} + u_{\beta,\alpha}^{(n)}, \\ 2\varepsilon_{\alpha 3}^{(n)} &= \beta_{\alpha}^{(n)} + u_{3,\alpha}^{(n)}, \quad \varepsilon_{33}^{(n)} = \beta_{3}^{(n)}, \end{aligned} \tag{1}$$

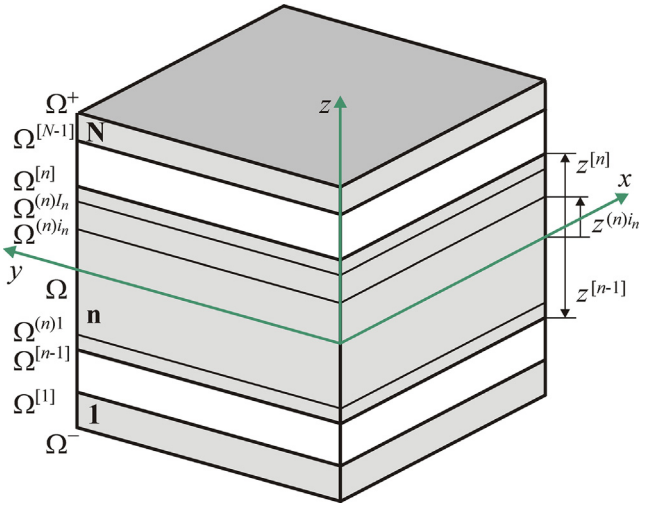

Fig. 1. Geometry of the laminated rectangular plate.

where $u_i^{(n)}$ are the displacements of the nth layer; $\beta_i^{(n)}$ are the derivatives of displacements with respect to the transverse coordinate:

$$\beta_i^{(n)} = u_{i,3}^{(n)}. \tag{2}$$

The constitutive equations in the case of linear elastic materials are defined as

$$\sigma_{ij}^{(n)} = C_{ijkl}^{(n)} \varepsilon_{kl}^{(n)} \tag{3}$$

where $\sigma_{ij}^{(n)}$ are the stresses of the nth layer; $C_{ijkl}^{(n)}$ are the elastic constants of the nth layer. Here and throughout the paper, Latin indices $i,\ j,\ k,\ l$ range from 1 to 3, whereas Greek indices $\alpha,\ \beta$ range from 1 to 2 and, as usual, summation on repeated tensorial indices is implied.

The equilibrium equations are written as

$$\sigma_{ij,j}^{(n)} = 0, \tag{4}$$

where $(\ldots)_{,i}$ stands for the partial derivatives with respect to Cartesian coordinates.

The boundary conditions on the edge surfaces $x = 0$ and $x = a$ are defined as

$$\begin{aligned} u_i^{(n)}(0, y, z) &= v_{1i}^{(n)-}(y, z) \ \text{ or } \ \sigma_{1i}^{(n)}(0, y, z) = p_{1i}^{(n)-}(y, z), \\ u_i^{(n)}(a, y, z) &= v_{1i}^{(n)+}(y, z) \ \text{ or } \ \sigma_{1i}^{(n)}(a, y, z) = p_{1i}^{(n)+}(y, z), \end{aligned} \tag{5}$$

where $v_{1i}^{(n)-}$, $v_{1i}^{(n)+}$ and $p_{1i}^{(n)-}$, $p_{1i}^{(n)+}$ are the prescribed displacements and mechanical loads acting on the nth layer.

The boundary conditions on the edge surfaces $y = 0$ and $y = b$ are written as

$$\begin{aligned} u_i^{(n)}(x, 0, z) &= v_{2i}^{(n)-}(x, z) \ \text{ or } \ \sigma_{2i}^{(n)}(x, 0, z) = p_{2i}^{(n)-}(x, z), \\ u_i^{(n)}(x, b, z) &= v_{2i}^{(n)+}(x, z) \ \text{ or } \ \sigma_{2i}^{(n)}(x, b, z) = p_{2i}^{(n)+}(x, z), \end{aligned} \tag{6}$$

where $v_{2i}^{(n)-}$, $v_{2i}^{(n)+}$ and $p_{2i}^{(n)-}$, $p_{2i}^{(n)+}$ are the prescribed displacements and mechanical loads acting on the nth layer.

The boundary conditions on the bottom and top surfaces are given by

$$\begin{aligned} u_i^{(1)}(x, y, -h/2) &= v_{3i}^{-}(x, y) \ \text{ or } \ \sigma_{3i}^{(1)}(x, y, -h/2) = p_{3i}^{-}(x, y), \\ u_i^{(N)}(x, y, h/2) &= v_{3i}^{+}(x, y) \ \text{ or } \ \sigma_{3i}^{(N)}(x, y, h/2) = p_{3i}^{+}(x, y), \end{aligned} \tag{7}$$

where v_{3i}^{-}, v_{3i}^{+} and p_{3i}^{-}, p_{3i}^{+} are the prescribed displacements and mechanical loads acting on the outer surfaces Ω^{-} and Ω^{+}.

The continuity conditions at interfaces $\Omega^{[m]}$ are

$$u_i^{(m)}(z^{[m]}) = u_i^{(m+1)}(z^{[m]}), \tag{8}$$

$$\sigma_{i3}^{(m)}(z^{[m]}) = \sigma_{i3}^{(m+1)}(z^{[m]}), \tag{9}$$

where the index m identifies the belonging of any quantity to the interface and runs from 1 to $N-1$.

3. Strong SaS formulation for laminated rectangular plate

According to the SaS concept [26], within the nth layer, we choose I_n SaS $\Omega^{(n)1}$, $\Omega^{(n)2}, \ldots, \Omega^{(n)I_n}$ parallel to the middle surface and located at the Chebyshev polynomial nodes (see Fig. 1). The coordinates of SaS of the nth layer are written as

$$\begin{aligned} z^{(n)i_n} &= \tfrac{1}{2}(z^{[n-1]} + z^{[n]}) - \tfrac{1}{2}h_n \cos\left(\pi \tfrac{2i_n - 1}{2I_n}\right), \\ h_n &= z^{[n]} - z^{[n-1]}, \end{aligned} \tag{10}$$

where $z^{[n-1]}$ and $z^{[n]}$ are the coordinates of interfaces $\Omega^{[n-1]}$ and $\Omega^{[n]}$; the indices i_n and j_n, k_n used later identify the belonging of any quantity to the SaS of the nth layer and run from 1 to I_n. So, in the strong SaS formulation the total number of SaS is $N_{\mathrm{SaS}} = \sum_n I_n$.

Introduce displacements $u_i^{(n)i_n}(x, y)$, strains $\varepsilon_{ij}^{(n)i_n}(x, y)$ and stresses $\sigma_{ij}^{(n)i_n}(x, y)$ of SaS of the nth layer as follows:

$$u_i^{(n)i_n} = u_i^{(n)}(z^{(n)i_n}), \tag{11}$$

$$\varepsilon_{ij}^{(n)i_n} = \varepsilon_{ij}^{(n)}(z^{(n)i_n}), \tag{12}$$

$$\sigma_{ij}^{(n)i_n} = \sigma_{ij}^{(n)}(z^{(n)i_n}). \tag{13}$$

Using Eqs. (1), (2), (11) and (12) leads to strain–displacement relations in terms of the SaS variables

$$\begin{aligned} 2\varepsilon_{\alpha\beta}^{(n)i_n} &= u_{\alpha,\beta}^{(n)i_n} + u_{\beta,\alpha}^{(n)i_n}, \\ 2\varepsilon_{\alpha 3}^{(n)i_n} &= \beta_{\alpha}^{(n)i_n} + u_{3,\alpha}^{(n)i_n}, \quad \varepsilon_{33}^{(n)i_n} = \beta_3^{(n)i_n}, \end{aligned} \tag{14}$$

where $\beta_i^{(n)i_n}(x, y)$ are the values of derivatives of the displacements of the nth layer with respect to the thickness coordinate at SaS:

$$\beta_i^{(n)i_n} = \beta_i^{(n)}(z^{(n)i_n}). \tag{15}$$

From Eqs. (3), (12) and (13) follow constitutive equations in terms of the SaS variables

$$\sigma_{ij}^{(n)i_n} = C_{ijkl}^{(n)} \varepsilon_{kl}^{(n)i_n} \tag{16}$$

The fundamental assumption of the strong SaS formulation [26] is that the displacements are distributed through the thickness of the nth layer by

$$u_i^{(n)} = \sum_{i_n} L^{(n)i_n} u_i^{(n)i_n}, \tag{17}$$

where $L^{(n)i_n}(z)$ are the Lagrange basis polynomials of degree $I_n - 1$ related to the nth layer:

$$L^{(n)i_n} = \prod_{j_n \neq i_n} \frac{z - z^{(n)j_n}}{z^{(n)i_n} - z^{(n)j_n}}. \tag{18}$$

Substituting the displacement distribution (17) in Eqs. (2) and (15), we obtain

$$\beta_i^{(n)i_n} = \sum_{j_n} M^{(n)j_n}(z^{(n)i_n}) u_i^{(n)j_n}, \tag{19}$$

where $M^{(n)j_n} = L_{,3}^{(n)j_n}$ are the derivatives of the Lagrange basis polynomials; their values on SaS are calculated as follows:

$$\begin{aligned} M^{(n)j_n}\left(x_3^{(n)i_n}\right) &= \frac{1}{x_3^{(n)j_n} - x_3^{(n)i_n}} \prod_{k_n \neq i_n, j_n} \frac{z^{(n)i_n} - z^{(n)k_n}}{z^{(n)j_n} - z^{(n)k_n}} \quad \text{for } j_n \neq i_n, \\ M^{(n)i_n}\left(z^{(n)i_n}\right) &= -\sum_{j_n \neq i_n} M^{(n)j_n}\left(z^{(n)i_n}\right). \end{aligned} \tag{20}$$

Proposition 1. The strains are distributed through the thickness of the nth layer by

$$\varepsilon_{ij}^{(n)} = \sum_{i_n} L^{(n)i_n} \varepsilon_{ij}^{(n)i_n}. \tag{21}$$

The proof of the proposition can be found in paper [26].

Proposition 2. The stresses are distributed through the thickness of the nth layer by

$$\sigma_{ij}^{(n)} = \sum_{i_n} L^{(n)i_n} \sigma_{ij}^{(n)i_n}. \tag{22}$$

This proposition can be proved using constitutive equations (3) and (16), and strain distribution (21).

Satisfying equilibrium equations (4) at the inner SaS of each layer, we arrive at $3(N_{\mathrm{SaS}} - 2N)$ differential equations

$$\sigma_{i1,1}^{(n)}(z^{(n)r_n}) + \sigma_{i2,2}^{(n)}(z^{(n)r_n}) + \sigma_{i3,3}^{(n)}(z^{(n)r_n}) = 0, \tag{23}$$

which can be expressed using Eqs. (13) and (22) in the following form:

$$\sigma_{i1,1}^{(n)r_n} + \sigma_{i2,2}^{(n)r_n} + \sum_{i_n} M^{(n)i_n}(z^{(n)r_n}) \sigma_{i3}^{(n)i_n} = 0, \tag{24}$$

where the index r_n identifies the belonging of any quantity to the inner SaS of the nth layer and runs from 2 to $I_n - 1$.

Next, we satisfy boundary conditions (7) that results in

$$\sum_{i_1} L^{(1)i_1}(-h/2) u_i^{(1)i_1} = v_{3i}^{-}(x, y) \;\text{ or }\; \sum_{i_1} L^{(1)i_1}(-h/2) \sigma_{3i}^{(1)i_1} = p_{3i}^{-}(x, y), \tag{25}$$

$$\sum_{i_N} L^{(N)i_N}(h/2) u_i^{(N)i_N} = v_{3i}^{+}(x, y) \;\text{ or }\; \sum_{i_N} L^{(N)i_N}(h/2) \sigma_{3i}^{(N)i_N} = p_{3i}^{+}(x, y), \tag{26}$$

and continuity conditions (8) and (9) at interfaces $\Omega^{[m]}$:

$$\sum_{i_m} L^{(m)i_m}(z^{[m]}) u_i^{(m)i_m} = \sum_{i_{m+1}} L^{(m+1)i_{m+1}}(z^{[m]}) u_i^{(m+1)i_{m+1}}, \tag{27}$$

$$\sum_{i_m} L^{(m)i_m}(z^{[m]}) \sigma_{i3}^{(m)i_m} = \sum_{i_{m+1}} L^{(m+1)i_{m+1}}(z^{[m]}) \sigma_{i3}^{(m+1)i_{m+1}}. \tag{28}$$

The boundary conditions (5) and (6) on the edge surfaces are satisfied at points $z^{(n)i_n}$, that is, for all SaS:

$$\begin{aligned} u_i^{(n)i_n}(0, y) &= v_{1i}^{(n)-}(y, z^{(n)i_n}) \;\text{ or }\; \sigma_{1i}^{(n)i_n}(0, y) = p_{1i}^{(n)-}(y, z^{(n)i_n}), \\ u_i^{(n)i_n}(a, y) &= v_{1i}^{(n)+}(y, z^{(n)i_n}) \;\text{ or }\; \sigma_{1i}^{(n)i_n}(a, y) = p_{1i}^{(n)+}(y, z^{(n)i_n}), \end{aligned} \tag{29}$$

$$\begin{aligned} u_i^{(n)i_n}(x, 0) &= v_{2i}^{(n)-}(x, z^{(n)i_n}) \;\text{ or }\; \sigma_{2i}^{(n)i_n}(x, 0) = p_{2i}^{(n)-}(x, z^{(n)i_n}), \\ u_i^{(n)i_n}(x, b) &= v_{2i}^{(n)+}(x, z^{(n)i_n}) \;\text{ or }\; \sigma_{2i}^{(n)i_n}(x, b) = p_{2i}^{(n)+}(x, z^{(n)i_n}). \end{aligned} \tag{30}$$

Thus, the proposed strong SaS formulation deals with $3N_{\mathrm{SaS}}$ governing equations (24) to (28) for finding the same number of SaS displacements $u_i^{(n)i_n}$. These equations should be solved to describe the response of the laminated composite plate with boundary conditions (29) and (30). For this purpose, the extended DQ method [58] can be effectively applied.

4. Extended DQ method for laminated rectangular plate

To solve the boundary value problem (24)-(30), the EDQ method can be employed using the Chebyshev-Gauss-Lobatto grid (Fig. 2):

$$x_{n_1} = \frac{1}{2}a\left[1 - \cos\left(\pi \frac{n_1 - 1}{N_1 - 1}\right)\right], \quad y_{n_2} = \frac{1}{2}b\left[1 - \cos\left(\pi \frac{n_2 - 1}{N_2 - 1}\right)\right], \tag{31}$$

where $n_1 = 1, 2, \ldots, N_1$; $n_2 = 1, 2, \ldots, N_2$; N_1 is the number of points in x-axis; N_2 is the number of points in y-axis.

To implement the EDQ method, we introduce the nodal displacements, strains and stresses of SaS of the nth layer by

$$u_{in_1 n_2}^{(n)i_n} = u_i^{(n)i_n}(x_{n_1}, y_{n_2}), \tag{32}$$

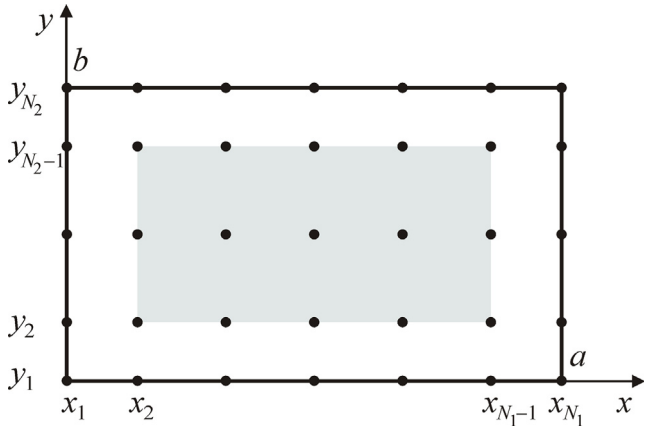

Fig. 2. Chebyshev-Gauss-Lobatto grid for the rectangular domain.

$$\varepsilon_{ijn_1n_2}^{(n)i_n} = \varepsilon_{ij}^{(n)i_n}(x_{n_1}, y_{n_2}), \tag{33}$$

$$\sigma_{ijn_1n_2}^{(n)i_n} = \sigma_{ij}^{(n)i_n}(x_{n_1}, y_{n_2}). \tag{34}$$

The in-plane distributions of displacements, strains and stresses of SaS can be written as

$$u_i^{(n)i_n} = \sum_{n_1}\sum_{n_2} L_{n_1}(x)L_{n_2}(y)u_{in_1n_2}^{(n)i_n}, \tag{35}$$

$$\varepsilon_{ij}^{(n)i_n} = \sum_{n_1}\sum_{n_2} L_{n_1}(x)L_{n_2}(y)\varepsilon_{ijn_1n_2}^{(n)i_n}, \tag{36}$$

$$\sigma_{ij}^{(n)i_n} = \sum_{n_1}\sum_{n_2} L_{n_1}(x)L_{n_2}(y)\sigma_{ijn_1n_2}^{(n)i_n}, \tag{37}$$

where $L_{n_1}(x)$, $L_{n_2}(y)$ are the Lagrange basis polynomials defined as

$$L_{n_1}(x) = \prod_{k_1\neq n_1} \frac{x - x_{k_1}}{x_{n_1} - x_{k_1}}, \tag{38}$$

$$L_{n_2}(y) = \prod_{k_2\neq n_2} \frac{y - y_{k_2}}{y_{n_2} - y_{k_2}}, \tag{39}$$

where $k_1 = 1, 2, \ldots, N_1$; $k_2 = 1, 2, \ldots, N_2$.

Using Eqs. (14), (19), (33) and (35) leads to strain–displacement relations in terms of the nodal SaS variables

$$\begin{aligned} 2\varepsilon_{\alpha\beta\, n_1n_2}^{(n)i_n} &= \omega_{\alpha\beta\, n_1n_2}^{(n)i_n} + \omega_{\beta\alpha\, n_1n_2}^{(n)i_n}, \\ 2\varepsilon_{\alpha 3n_1n_2}^{(n)i_n} &= \beta_{\alpha\, n_1n_2}^{(n)i_n} + \omega_{3\alpha\, n_1n_2}^{(n)i_n}, \quad \varepsilon_{33n_1n_2}^{(n)i_n} = \beta_{3n_1n_2}^{(n)i_n}, \end{aligned} \tag{40}$$

where

$$\begin{aligned} \omega_{i1n_1n_2}^{(n)i_n} &= \textstyle\sum_{k_1} M_{k_1}(x_{n_1})u_{ik_1n_2}^{(n)i_n}, \quad \omega_{i2n_1n_2}^{(n)i_n} = \textstyle\sum_{k_2} M_{k_2}(y_{n_2})u_{in_1k_2}^{(n)i_n}, \\ \beta_{in_1n_2}^{(n)i_n} &= \textstyle\sum_{j_n} M^{(n)j_n}(z^{(n)i_n})u_{in_1n_2}^{(n)j_n}, \end{aligned} \tag{41}$$

where $M_{k_1}(x)$ and $M_{k_2}(y)$ are the derivatives of the Lagrange basis polynomials (38) and (39) whose values at the grid points are calculated as

$$\begin{aligned} M_{k_1}(x_{n_1}) &= \tfrac{1}{x_{k_1} - x_{n_1}} \prod_{l_1\neq k_1,\, n_1} \tfrac{x_{n_1} - x_{l_1}}{x_{k_1} - x_{l_1}} \quad \text{for } k_1 \neq n_1, \\ M_{n_1}(x_{n_1}) &= -\textstyle\sum_{k_1\neq n_1} M_{k_1}(x_{n_1}), \end{aligned} \tag{42}$$

$$\begin{aligned} M_{k_2}(y_{n_2}) &= \tfrac{1}{y_{k_2} - y_{n_2}} \prod_{l_2\neq k_2,\, n_2} \tfrac{y_{n_2} - y_{l_2}}{y_{k_2} - y_{l_2}} \quad \text{for } k_2 \neq n_2, \\ M_{n_2}(y_{n_2}) &= -\textstyle\sum_{k_2\neq n_2} M_{k_2}(y_{n_2}). \end{aligned} \tag{43}$$

Constitutive equations (16) owing to Eqs. (33) and (34) are expressed in terms of the nodal SaS variables as

$$\sigma_{ijn_1n_2}^{(n)i_n} = C_{ijkl}^{(n)}\varepsilon_{kln_1n_2}^{(n)i_n}. \tag{44}$$

Substituting Eq. (37) into equilibrium equations (24) and satisfying them in the inner rectangle (see Fig. 2), we obtain $3(N_1-2)(N_2-2)(N_{\text{SaS}}-2N)$ algebraic equations

$$\sum_{n_1} M_{n_1}(x_{s_1})\,\sigma_{i1n_1s_2}^{(n)r_n} + \sum_{n_2} M_{n_2}(y_{s_2})\,\sigma_{i2s_1n_2}^{(n)r_n} + \sum_{i_n} M^{(n)i_n}(z^{(n)r_n})\sigma_{i3s_1s_2}^{(n)i_n} = 0. \tag{45}$$

Here and below, the indices s_1 and s_2 identify the belonging of any quantity to the inner grid points and run respectively from 2 to $N_1 - 1$ and from 2 to $N_2 - 1$.

Introduce the global vector of SaS displacements at the grid points

$$\boldsymbol{U} = \left[(\boldsymbol{U}^{(1)1})^{\mathrm{T}}(\boldsymbol{U}^{(1)2})^{\mathrm{T}}\ldots(\boldsymbol{U}^{(1)I_1})^{\mathrm{T}}\ldots(\boldsymbol{U}^{(n)1})^{\mathrm{T}}(\boldsymbol{U}^{(n)2})^{\mathrm{T}}\ldots(\boldsymbol{U}^{(n)I_n})^{\mathrm{T}}\ldots(\boldsymbol{U}^{(N)1})^{\mathrm{T}}(\boldsymbol{U}^{(N)2})^{\mathrm{T}}\ldots(\boldsymbol{U}^{(N)I_N})^{\mathrm{T}}\right]^{\mathrm{T}}, \tag{46}$$

$$\boldsymbol{U}^{(n)i_n} = \left[(\boldsymbol{u}_{11}^{(n)i_n})^{\mathrm{T}}(\boldsymbol{u}_{21}^{(n)i_n})^{\mathrm{T}}\ldots(\boldsymbol{u}_{N_11}^{(n)i_n})^{\mathrm{T}}(\boldsymbol{u}_{12}^{(n)i_n})^{\mathrm{T}}(\boldsymbol{u}_{22}^{(n)i_n})^{\mathrm{T}}\ldots(\boldsymbol{u}_{N_12}^{(n)i_n})^{\mathrm{T}}\ldots(\boldsymbol{u}_{1N_2}^{(n)i_n})^{\mathrm{T}}(\boldsymbol{u}_{2N_2}^{(n)i_n})^{\mathrm{T}}\ldots(\boldsymbol{u}_{N_1N_2}^{(n)i_n})^{\mathrm{T}}\right]^{\mathrm{T}}, \tag{47}$$

where

$$\boldsymbol{u}_{n_1n_2}^{(n)i_n} = \left[u_{1n_1n_2}^{(n)i_n}\; u_{2n_1n_2}^{(n)i_n}\; u_{3n_1n_2}^{(n)i_n}\right]^{\mathrm{T}}. \tag{48}$$

Then the strain–displacement relations (40) and (41) are written in matrix form as

$$2\boldsymbol{\varepsilon}_{ijn_1n_2}^{(n)i_n} = \left(\boldsymbol{\Lambda}_{ijn_1n_2}^{(n)i_n} + \boldsymbol{\Lambda}_{jin_1n_2}^{(n)i_n}\right)^{\mathrm{T}}\boldsymbol{U}, \tag{49}$$

where $\boldsymbol{\Lambda}_{ijn_1n_2}^{(n)i_n}$ are the vectors of order $3N_1N_2N_{\text{SaS}}$ given in Appendix A.

Constitutive equations (44) can be also expressed in matrix form as

$$\boldsymbol{\sigma}_{ijn_1n_2}^{(n)i_n} = \left(\boldsymbol{\Xi}_{ijn_1n_2}^{(n)i_n}\right)^{T}\boldsymbol{U}. \tag{50}$$

where $\boldsymbol{\Xi}_{ijn_1n_2}^{(n)i_n}$ are the vectors defined as

$$\boldsymbol{\Xi}_{ijn_1n_2}^{(n)i_n} = C_{ijkl}^{(n)}\boldsymbol{\Lambda}_{kln_1n_2}^{(n)i_n}. \tag{51}$$

The use of Eqs. (50) and (51) in equilibrium equations (45) leads to

$$\left[\sum_{n_1} M_{n_1}(x_{s_1})\left(\boldsymbol{\Xi}_{i1n_1s_2}^{(n)r_n}\right)^{\mathrm{T}} + \sum_{n_2} M_{n_2}(y_{s_2})\left(\boldsymbol{\Xi}_{i2s_1n_2}^{(n)r_n}\right)^{\mathrm{T}} + \sum_{i_n} M^{(n)i_n}(z^{(n)r_n})\left(\boldsymbol{\Xi}_{i3s_1s_2}^{(n)i_n}\right)^{\mathrm{T}}\right]\boldsymbol{U} = 0. \tag{52}$$

Boundary conditions (25) and (26) on the outer surfaces Ω^- and Ω^+ are satisfied at the grid points (x_{n_1}, y_{n_2}):

$$\begin{aligned} &\sum_{i_1} L^{(1)i_1}(-h/2)\left[\alpha_{3i}^-\left(\boldsymbol{\Xi}_{3in_1n_2}^{(1)i_1}\right)^{\mathrm{T}} + (1-\alpha_{3i}^-)\left(\boldsymbol{\Gamma}_{in_1n_2}^{(1)i_1}\right)^{\mathrm{T}}\right]\boldsymbol{U} \\ &\quad = \alpha_{3i}^- p_{3i}^-(x_{n_1}, y_{n_2}) + (1-\alpha_{3i}^-)v_{3i}^-(x_{n_1}, y_{n_2}), \end{aligned} \tag{53}$$

$$\begin{aligned} &\sum_{i_N} L^{(N)i_N}(h/2)\left[\alpha_{3i}^+\left(\boldsymbol{\Xi}_{3in_1n_2}^{(N)i_N}\right)^{\mathrm{T}} + (1-\alpha_{3i}^+)\left(\boldsymbol{\Gamma}_{in_1n_2}^{(N)i_N}\right)^{\mathrm{T}}\right]\boldsymbol{U} \\ &\quad = \alpha_{3i}^+ p_{3i}^+(x_{n_1}, y_{n_2}) + (1-\alpha_{3i}^+)v_{3i}^+(x_{n_1}, y_{n_2}), \end{aligned} \tag{54}$$

where $\boldsymbol{\Gamma}_{in_1n_2}^{(n)i_n}$ are the nodal vectors given in Appendix A. Hereinafter, summation on the repeated indices is not implied.

Continuity conditions (27) and (28) at the interfaces $\Omega^{[m]}$ are also satisfied at the grid points (x_{n_1}, y_{n_2}):

$$\left[\sum_{i_m} L^{(m)i_m}(z^{[m]})\left(\boldsymbol{\Gamma}_{in_1n_2}^{(m)i_m}\right)^{\mathrm{T}} - \sum_{i_{m+1}} L^{(m+1)i_{m+1}}(z^{[m]})\left(\boldsymbol{\Gamma}_{in_1n_2}^{(m+1)i_{m+1}}\right)^{\mathrm{T}}\right]\boldsymbol{U} = 0, \tag{55}$$

$$\left[\sum_{i_m} L^{(m)i_m}(z^{[m]})\left(\boldsymbol{\Xi}_{i3n_1n_2}^{(m)i_m}\right)^{\mathrm{T}} - \sum_{i_{m+1}} L^{(m+1)i_{m+1}}(z^{[m]})\left(\boldsymbol{\Xi}_{i3n_1n_2}^{(m+1)i_{m+1}}\right)^{\mathrm{T}}\right]\boldsymbol{U} = 0. \tag{56}$$

The boundary conditions on the edge surfaces (29) are satisfied for *inner* SaS of the nth layer $\Omega^{(n)r_n}$ at the grid points $(0, y_{s_2})$ and (a, y_{s_2}):

$$\left[\alpha_{1i}^{-}\left(\boldsymbol{\Xi}_{1i1s_2}^{(n)r_n}\right)^{\mathrm{T}}+(1-\alpha_{1i}^{-})\left(\boldsymbol{\Gamma}_{i1s_2}^{(n)r_n}\right)^{\mathrm{T}}\right]\boldsymbol{U}$$
$$=\alpha_{1i}^{-}p_{1i}^{(n)-}(y_{s_2},z^{(n)r_n})+(1-\alpha_{1i}^{-})v_{1i}^{(n)-}(y_{s_2},z^{(n)r_n}),\tag{57}$$

$$\left[\alpha_{1i}^{+}\left(\boldsymbol{\Xi}_{1iN_1s_2}^{(n)r_n}\right)^{\mathrm{T}}+(1-\alpha_{1i}^{+})\left(\boldsymbol{\Gamma}_{iN_1s_2}^{(n)r_n}\right)^{\mathrm{T}}\right]\boldsymbol{U}$$
$$=\alpha_{1i}^{+}p_{1i}^{(n)+}(y_{s_2},z^{(n)r_n})+(1-\alpha_{1i}^{+})v_{1i}^{(n)+}(y_{s_2},z^{(n)r_n}).\tag{58}$$

The boundary conditions on the edge surfaces (30) are satisfied for *inner* SaS of the nth layer $\Omega^{(n)r_n}$ at the grid points $(x_{n_1},0)$ and (x_{n_1},b):

$$\left[\alpha_{2i}^{-}\left(\boldsymbol{\Xi}_{2in_1 1}^{(n)r_n}\right)^{\mathrm{T}}+(1-\alpha_{2i}^{-})\left(\boldsymbol{\Gamma}_{in_1 1}^{(n)r_n}\right)^{\mathrm{T}}\right]\boldsymbol{U}$$
$$=\alpha_{2i}^{-}p_{2i}^{(n)-}(x_{n_1},z^{(n)r_n})+(1-\alpha_{2i}^{-})v_{2i}^{(n)-}(x_{n_1},z^{(n)r_n}),\tag{59}$$

$$\left[\alpha_{2i}^{+}\left(\boldsymbol{\Xi}_{2in_1N_2}^{(n)r_n}\right)^{\mathrm{T}}+(1-\alpha_{2i}^{+})\left(\boldsymbol{\Gamma}_{in_1N_2}^{(n)r_n}\right)^{\mathrm{T}}\right]\boldsymbol{U}$$
$$=\alpha_{2i}^{+}p_{2i}^{(n)+}(x_{n_1},z^{(n)r_n})+(1-\alpha_{2i}^{+})v_{2i}^{(n)+}(x_{n_1},z^{(n)r_n}).\tag{60}$$

Remark 1. To describe the boundary conditions for displacements and stresses in Eqs. (53), (54), (57) to (60), we introduce coefficients α_{ij}^{-} and α_{ij}^{+}, which take values 0 or 1.

The system of algebraic equations (52)-(60) can be written in a compact form as

$$\boldsymbol{KU}=\boldsymbol{F}\tag{61}$$

where $\boldsymbol{K}$ is the stiffness matrix; $\boldsymbol{F}$ is the right-hand side vector.

It is seen that the SaS/EDQ formulation deals with $3N_1N_2N_{\mathrm{SaS}}$ algebraic equations (61) for obtaining the SaS displacements at the grid points $u_{in_1n_2}^{(n)i_n}$. The strains and stresses are calculated by Eqs. (49) and (50). The numerical examples considered in the next section were solved using C++ OpenMP, which is the most popular parallel computing technology for multi-processor/core computers. As an algebra solver, we employ the UMFPACK library [59,60] based on solving sparse unsymmetric linear systems using the multifrontal method [61].

5. Numerical examples

In this section, the cross-ply and angle-ply composite rectangular plates with arbitrary boundary conditions are studied. To identify them, the standard notations are used, for example, the $\mathrm{CSC_1F}$ plate means that the edge $x=0$ is clamped

$$u_1^{(n)r_n}=u_2^{(n)r_n}=u_3^{(n)r_n}=0,\tag{62}$$

the edge $y=0$ is simply supported

$$u_1^{(n)r_n}=\sigma_{22}^{(n)r_n}=u_3^{(n)r_n}=0,\tag{63}$$

the edge $x=a$ is clamped in x- and z-directions

$$u_1^{(n)r_n}=\sigma_{12}^{(n)r_n}=u_3^{(n)r_n}=0,\tag{64}$$

the edge $y=b$ is free

$$\sigma_{12}^{(n)r_n}=\sigma_{22}^{(n)r_n}=\sigma_{23}^{(n)r_n}=0.\tag{65}$$

5.1. Cross-ply laminates with arbitrary boundary conditions

Here, we study a three-ply composite rectangular plate with the lamination scheme [0/90/0] and ply thicknesses $h_1=h_2=h_3=h/3$. The fibers of the unidirectional graphite-epoxy composite in the outer layers are oriented along the x-axis. The material properties are taken to be $E_{\mathrm{L}}=25E_{\mathrm{T}}$, $G_{\mathrm{LT}}=0.5E_{\mathrm{T}}$, $G_{\mathrm{TT}}=0.2E_{\mathrm{T}}$, $E_{\mathrm{T}}=10^6$ and $\nu_{\mathrm{LT}}=\nu_{\mathrm{TT}}=0.25$. The plate is subjected to a sinusoidally distributed load on the top surface

$$p_{31}^{+}=p_{32}^{+}=0,\quad p_{33}^{+}=p_0\sin\frac{\pi x}{a}\sin\frac{\pi y}{b},\tag{66}$$

where $p_0=1$.

For verification, we consider the simplest SSSS laminate [2] and introduce the dimensionless variables at crucial points as functions of the dimensionless thickness coordinate as

$$\bar{u}_1=100E_{\mathrm{T}}h^2u_1(0,b/2,\bar{z})/a^3p_0,\quad \bar{u}_2$$
$$=100E_{\mathrm{T}}h^2u_2(a/2,0,\bar{z})/a^3p_0,\tag{67}$$

$$\bar{u}_3=100E_{\mathrm{T}}h^3u_3(a/2,b/2,\bar{z})/a^4p_0,\quad \bar{\sigma}_{11}=10h^2\sigma_{11}(a/2,b/2,\bar{z})/a^2p_0,$$

$$\bar{\sigma}_{22}=100h^2\sigma_{22}(a/2,b/2,\bar{z})/a^2p_0,\quad \bar{\sigma}_{12}=100h^2\sigma_{12}(0,0,\bar{z})/a^2p_0,$$

$$\bar{\sigma}_{13}=10h\sigma_{13}(0,b/2,\bar{z})/ap_0,\quad \bar{\sigma}_{23}=100h\sigma_{23}(a/2,0,\bar{z})/ap_0,$$

$$\bar{\sigma}_{33}=\sigma_{33}(a/2,b/2,\bar{z})/p_0,\quad \bar{z}=z/h,$$

where $a=1$.

Tables 1 and 2 list the results of the convergence study due to increasing the number of grid points. The number of SaS in each layer is fixed to nine, that is, the total number of SaS is $N_{\mathrm{SaS}}=27$. A comparison with the closed-form solution of Pagano [2], reproduced later in work [26], is also given. As can be seen, the use of a relatively coarse grid 13×13 provides from 9 to 10 right digits for the moderately thick plates. Fig. 3 shows the through-thickness distributions of displacements and stresses for the rectangular plate with $b/a=2$ for different values of the slenderness ratio a/h using nine SaS in each layer and 13×13 grid. These results convincingly demonstrate the high potential of the developed SaS/EDQ formulation, since the boundary conditions on the bottom and top surfaces and the continuity conditions at the interfaces for the transverse stresses are satisfied excellently.

Next, we consider CSCS, $\mathrm{C_1SC_1S}$ and FSFS laminates with Levy-type boundary conditions. To compare the obtained results with results of the analytical study [32], we introduce dimensionless variables as functions of the thickness coordinate:

$$\bar{u}_1=100E_{\mathrm{T}}h^2u_1(a/4,b/2,\bar{z})/a^3p_0,\quad \bar{u}_2$$
$$=100E_{\mathrm{T}}h^2u_2(a/2,b/4,\bar{z})/a^3p_0,\tag{68}$$

$$\bar{u}_3=100E_{\mathrm{T}}h^3u_3(a/2,b/2,\bar{z})/a^4p_0,\quad \bar{\sigma}_{11}=10h^2\sigma_{11}(a/2,b/2,\bar{z})/a^2p_0,$$

$$\bar{\sigma}_{22}=10h^2\sigma_{22}(a/2,b/2,\bar{z})/a^2p_0,\quad \bar{\sigma}_{12}=10h^2\sigma_{12}(a/8,0,\bar{z})/a^2p_0,$$

$$\bar{\sigma}_{13}=10h\sigma_{13}(a/8,b/2,\bar{z})/ap_0,\quad \bar{\sigma}_{23}=10h\sigma_{23}(a/2,0,\bar{z})/ap_0,$$

$$\bar{\sigma}_{33}=\sigma_{33}(a/2,b/2,\bar{z})/p_0,\quad \bar{z}=z/h,$$

where $a=b=1$.

Tables 3 and 4 show the results of the convergence study due to increasing the number of grid points using nine SaS in each layer for CSCS, $\mathrm{C_1SC_1S}$ and FSFS laminates. A comparison with the analytical solution of Vel-Batra [32] is presented. Fig. 4. displays the through-thickness distributions of displacements and stresses for the CSCS square laminate with various slenderness ratios using nine SaS in each layer and 13×13 grid. The results for the moderately thick plate with $a/h=5$ are compared with those obtained by Vel and Batra [32]. It is seen that again the boundary conditions on the outer surfaces and the continuity conditions at the interfaces for the transverse stresses are satisfied with high accuracy.

Table 1
Results of the convergence study for the SSSS laminate with $b/a = 1$ and nine SaS in each layer ($N_{SaS} = 27$).

a/h	$N_1 \times N_2$	$\bar{u}_1(0.5)$	$\bar{u}_2(0.5)$	$\bar{u}_3(0)$	$\bar{\sigma}_{11}(0.5)$	$\bar{\sigma}_{22}(0.5)$	$\bar{\sigma}_{12}(0.5)$	$\bar{\sigma}_{13}(0)$	$\bar{\sigma}_{23}(0)$	$\bar{\sigma}_{33}(0)$
4	7×7	−0.9687587335	−2.279949166	2.005441262	8.001624366	9.524029099	−5.104350539	2.558434832	21.72178649	0.4926472390
	9×9	−0.9694399339	−2.281217021	2.005915394	8.008389746	9.529924024	−5.106104003	2.559024611	21.71803346	0.4926507117
	11×11	−0.9694325813	−2.281203506	2.005911168	8.008404350	9.529952470	−5.106087322	2.559020377	21.71807432	0.4926507177
	13×13	−0.9694326293	−2.281203595	2.005911202	8.008404887	9.529952941	−5.106087440	2.559020412	21.71807409	0.4926507179
	SaS solution [a]	−0.9694326291	−2.281203594	2.005911202	8.008404888	9.529952942	−5.106087439	2.559020412	21.71807409	0.4926507179
	3D solution [b]	−0.9694319959	−2.281202598	2.005910531	8.008399824	9.529949306	−5.106084880	2.559019255	21.71807687	0.4926507131
10	7×7	−0.7344773595	−1.098745760	0.752705438	5.899787588	4.291169392	−2.879805743	3.572386050	12.27643531	0.4994436357
	9×9	−0.7351175406	−1.099479140	0.753032919	5.905908620	4.294672412	−2.881774098	3.573055875	12.27529462	0.4994443719
	11×11	−0.7351109242	−1.099471680	0.753030021	5.905914676	4.294683548	−2.881755645	3.573053315	12.27532184	0.4994443782
	13×13	−0.7351109699	−1.099471731	0.753030044	5.905915150	4.294683827	−2.881755768	3.573053347	12.27532184	0.4994443783
	SaS solution [a]	−0.7351109697	−1.099471731	0.753030044	5.905915152	4.294683828	−2.881755767	3.573053347	12.27532184	0.4994443783
	3D solution [b]	−0.7351109687	−1.099471730	0.753030043	5.905915143	4.294683823	−2.881755764	3.573053343	12.27532186	0.4994443783

[a] Exact results have been obtained using the SaS solution with nine SaS for each layer[26].
[b] Exact results have been obtained using the Pagano solution[2,26].

Table 2
Results of the convergence study for the SSSS cross-ply laminate with $a/h = 10$ and nine SaS in each layer ($N_{SaS} = 27$).

b/a	$N_1 \times N_2$	$\bar{u}_1(0.5)$	$\bar{u}_2(0.5)$	$\bar{u}_3(0)$	$\bar{\sigma}_{11}(0.5)$	$\bar{\sigma}_{22}(0.5)$	$\bar{\sigma}_{12}(0.5)$	$\bar{\sigma}_{13}(0)$	$\bar{\sigma}_{23}(0)$	$\bar{\sigma}_{33}(0)$
2	7×7	−0.8933014993	−0.6723224449	0.8990665036	7.090031755	2.014947646	−1.757674552	4.136893116	3.076000900	0.5001267878
	9×9	−0.8940948290	−0.6727747757	0.8994652443	7.097546924	2.016538694	−1.759011640	4.137570690	3.074880128	0.5001275750
	11×11	−0.8940865599	−0.6727704772	0.8994615192	7.097552802	2.016540645	−1.758999347	4.137566709	3.074894146	0.5001275826
	13×13	−0.8940866176	−0.6727705057	0.8994615482	7.097553391	2.016540778	−1.758999426	4.137566744	3.074894141	0.5001275827
	SaS solution [a]	−0.8940866173	−0.6727705056	0.8994615481	7.097553391	2.016540778	−1.758999426	4.137566744	3.074894141	0.5001275827
	3D solution [b]	−0.8940866165	−0.6727705051	0.8994615475	7.097553384	2.016540777	−1.758999425	4.137566741	3.074894139	0.5001275827
4	7×7	−0.9226861090	−0.3426882872	0.9243946875	7.301626835	1.249279680	−0.900623603	4.218563210	0.999864816	0.5002939959
	9×9	−0.9235144248	−0.3429243127	0.9248118111	7.309448840	1.250275529	−0.901327353	4.219249538	0.997416176	0.5002947889
	11×11	−0.9235056323	−0.3429220138	0.9248077193	7.309453027	1.250275618	−0.901320457	4.219244345	0.997427616	0.5002947970
	13×13	−0.9235056929	−0.3429220281	0.9248077499	7.309453641	1.250275695	−0.901320500	4.219244381	0.997427619	0.5002947970
	SaS solution [a]	−0.9235056927	−0.3429220281	0.9248077499	7.309453641	1.250275695	−0.901320500	4.219244381	0.997427619	0.5002947970
	3D solution [b]	−0.9235056918	−0.3429220278	0.9248077492	7.309453634	1.250275694	−0.901320499	4.219244378	0.997427619	0.5002947970

[a] Exact results have been obtained using the SaS solution with nine SaS for each layer[26].
[b] Exact results have been obtained using the Pagano solution [2,26].

5.2. Angle-ply laminates under sinusoidal loading

Consider CCCC laminates with stacking sequences $[-45/45/-45]$ and $[-45/45/0]$, and equal ply thicknesses. The laminates at the top are subjected to a sinusoidally distributed load (66). The material properties of the graphite-epoxy composite are given in section 5.1.

Here, we utilize dimensionless variables (68) and introduce new ones:

$$\bar{u}_3 = 100E_T h^2 u_3(a/2, b/2, \bar{z})/a^3 p_0, \quad \bar{\sigma}_{12} = 10h^2\sigma_{12}(a/4, b/4, \bar{z})/a^2 p_0, \tag{69}$$

$$\bar{\sigma}_{13} = 10h\sigma_{13}(a/4, b/2, \bar{z})/ap_0, \quad \bar{\sigma}_{23} = 10h\sigma_{23}(a/2, b/4, \bar{z})/ap_0,$$

where $a = 1$ and $b = 0.5$.

Table 5 lists the results of the convergence study due to mesh refinement using nine SaS for each layer. The results are compared with those obtained with the SOLID45 element from the ANSYS package [62] using a fine $64 \times 64 \times 72$ mesh. This means that 24 elements are taken across the thickness of each layer. Figs. 5 and 6 show the through-thickness distributions of displacements and stresses for thick and thin laminates using nine SaS in each layer and 13×13 grid compared with the SOLID45 element. As can be seen, the boundary conditions on the bottom and top surfaces and the continuity conditions at the interfaces for the transverse stress components are satisfied excellently. However, the SOLID45 element describes worse boundary conditions and continuity conditions as well.

5.3. Angle-ply laminates under exponential loading

Finally, we study four-ply laminates with stacking sequences $[45/-45/0/90]$, $[0/90/-60/30]$ and $[-60/30/45/-45]$, and ply thicknesses $h_1 = h_2 = h_3 = h_4 = h/4$ with clamped and free edges subjected to an exponentially distributed load at the top (see Fig. 7)

$$p_{31}^{+} = p_{32}^{+} = 0, \quad p_{33}^{+} = p_0 e^{-10(x-a/2)^2} e^{-10(y-b/2)^2}, \tag{70}$$

where $p_0 = 1$ and $a = b = 1$. The material properties of the composite are given in section 5.1.

Figs. 8–10 show the distributions of dimensional stresses (68) and (69) through the thickness of the FCCC, FCFF and FCFC angle-ply laminates with $a/h = 5$ using nine SaS in each layer ($N_{SaS} = 36$) and 13×13 grid. These results demonstrate again the high potential of the SaS/EDQ formulation developed, since the boundary conditions on the outer surfaces and the continuity conditions at the interfaces for the transverse stresses are satisfied with high accuracy.

6. Conclusions

An effective SaS/EDQ formulation for the three-dimensional analysis of cross-ply and angle-ply laminates has been proposed by using the

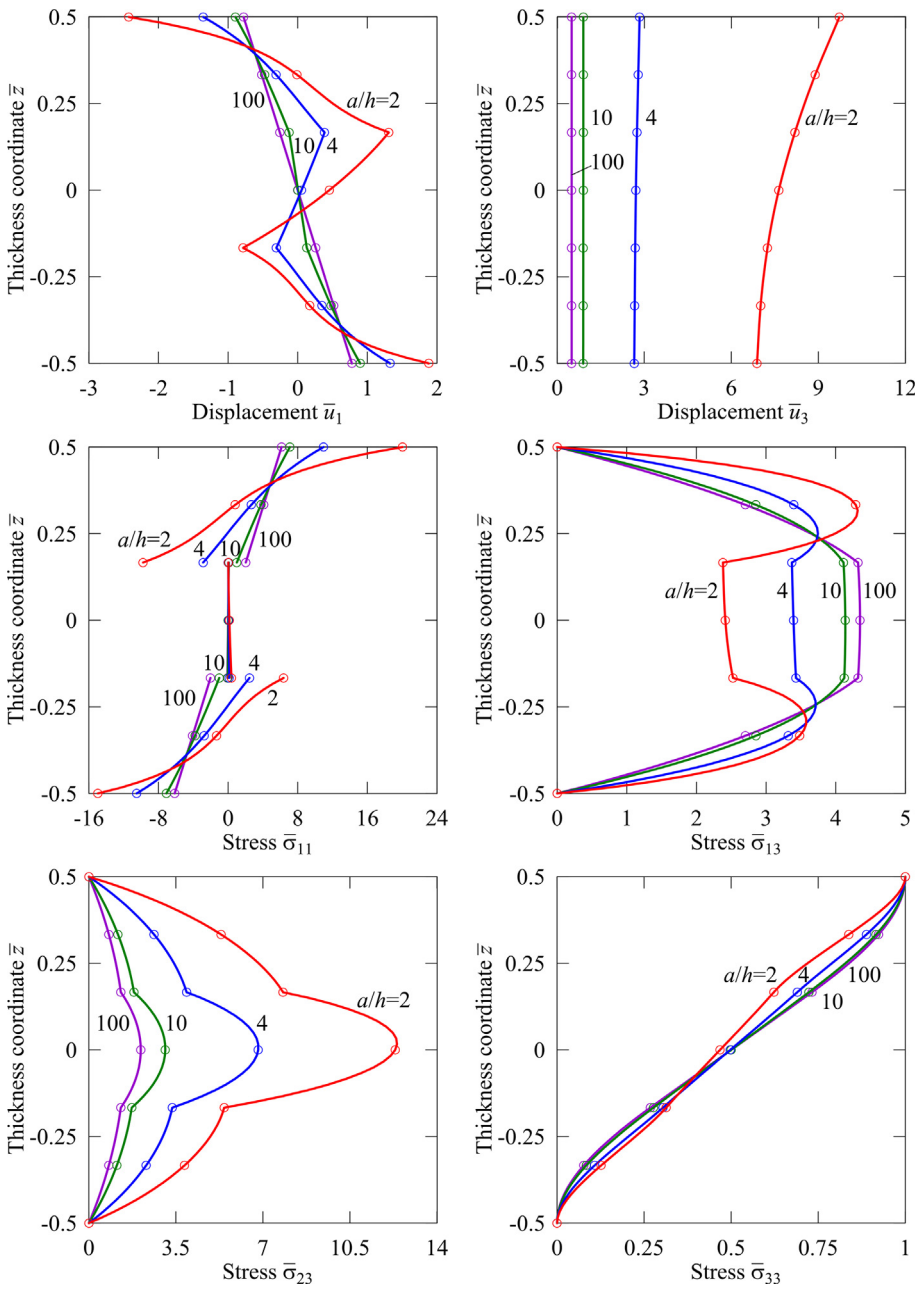

Fig. 3. Through-thickness distributions of displacements and stresses for the SSSS laminate with $b/a = 2$ under sinusoidal loading: SaS/EDQ formulation using nine SaS in each layer and 13×13 grid (solid lines) and Pagano solution (○) [26].

Table 3
Results of the convergence study for the CSCS cross-ply laminate with $b/a = 1$ and nine SaS in each layer ($N_{SaS} = 27$) [a].

a/h	$N_1 \times N_2$	$\overline{u}_1(-0.5)$	$\overline{u}_1(0.5)$	$\overline{u}_2(-0.5)$	$\overline{u}_2(0.5)$	$\overline{u}_3(0)$	$\overline{\sigma}_{11}(-0.5)$	$\overline{\sigma}_{11}(0.5)$	$\overline{\sigma}_{22}(-1/6)$	$\overline{\sigma}_{22}(1/6)$	$\overline{\sigma}_{12}(-0.5)$	$\overline{\sigma}_{12}(0.5)$	$\overline{\sigma}_{13}(0)$	$\overline{\sigma}_{23}(0)$	$\overline{\sigma}_{33}(0)$
5	7×7	0.3194	−0.3320	1.0526	−1.0435	1.1795	−4.1134	4.3742	−3.7234	3.5710	0.2581	−0.2585	2.0990	1.4702	0.4950
	9×9	0.3183	−0.3307	1.0535	−1.0443	1.1806	−4.2645	4.5334	−3.7282	3.5753	0.2560	−0.2563	2.0835	1.4710	0.4948
	11×11	0.3189	−0.3314	1.0534	−1.0442	1.1805	−4.2358	4.5050	−3.7282	3.5753	0.2563	−0.2566	2.0929	1.4705	0.4950
	13×13	0.3190	−0.3315	1.0534	−1.0442	1.1805	−4.2314	4.4997	−3.7280	3.5752	0.2565	−0.2569	2.0961	1.4709	0.4949
	3D solution	0.319	−0.331	1.053	−1.044	1.180	−4.235	4.504	−3.726	3.573	0.256	−0.257	2.093	1.470	0.495
10	7×7	0.2269	−0.2272	0.4642	−0.4590	0.4452	−2.8757	2.9053	−1.7093	1.6701	0.1265	−0.1255	3.1263	0.7204	0.4991
	9×9	0.2255	−0.2258	0.4654	−0.4601	0.4464	−3.0468	3.0794	−1.7139	1.6746	0.1238	−0.1229	3.0675	0.7225	0.4994
	11×11	0.2270	−0.2273	0.4651	−0.4598	0.4461	−2.9820	3.0139	−1.7131	1.6738	0.1241	−0.1232	3.0617	0.7217	0.4995
	13×13	0.2267	−0.2270	0.4652	−0.4599	0.4462	−3.0058	3.0376	−1.7132	1.6739	0.1245	−0.1235	3.0676	0.7221	0.4994
	3D solution	0.227	−0.227	0.465	−0.460	0.446	−3.000	3.032	−1.713	1.674	0.124	−0.123	3.062	0.722	0.50

[a] Values of the normal stress $\overline{\sigma}_{22}$correspond to the central layer

Table 4
Results of the convergence study for the C_1SC_1S and FSFS cross-ply laminates with $b/a = 1$, $a/h = 5$ and nine SaS in each layer ($N_{SaS} = 27$) [a].

Lamina	$N_1 \times N_2$	$\bar{u}_1(-0.5)$	$\bar{u}_1(0.5)$	$\bar{u}_2(-0.5)$	$\bar{u}_2(0.5)$	$\bar{u}_3(0)$	$\bar{\sigma}_{11}(-0.5)$	$\bar{\sigma}_{11}(0.5)$	$\bar{\sigma}_{22}(-1/6)$	$\bar{\sigma}_{22}(1/6)$	$\bar{\sigma}_{12}(-0.5)$	$\bar{\sigma}_{12}(0.5)$	$\bar{\sigma}_{13}(0)$	$\bar{\sigma}_{23}(0)$	$\bar{\sigma}_{33}(0)$
C_1SC_1S	7×7	0.3214	−0.3339	1.0615	−1.0523	1.1877	−4.1191	4.3790	−3.7556	3.6022	0.2188	−0.2210	2.1079	1.4757	0.4949
	9×9	0.3202	−0.3325	1.0613	−1.0521	1.1886	−4.2830	4.5514	−3.7548	3.6016	0.2217	−0.2241	2.0905	1.4793	0.4948
	11×11	0.3208	−0.3332	1.0613	−1.0520	1.1883	−4.2546	4.5230	−3.7550	3.6018	0.2208	−0.2231	2.1017	1.4783	0.4950
	13×13	0.3210	−0.3334	1.0613	−1.0520	1.1884	−4.2479	4.5156	−3.7547	3.6015	0.2205	−0.2225	2.1053	1.4787	0.4949
	3D solution	0.321	−0.333	1.061	−1.051	1.188	−4.253	4.520	−3.753	3.599	0.221	−0.223	2.102	1.478	0.495
FSFS	9×9	0.1085	−0.1143	5.0154	−5.0076	5.3077	−2.0674	2.2551	−17.249	17.103	0.0600	−0.0624	0.6528	5.9174	0.4963
	11×11	0.1083	−0.1140	5.0151	−5.0073	5.3074	−2.0363	2.2265	−17.247	17.102	0.0593	−0.0615	0.6114	5.9183	0.4960
	13×13	0.1078	−0.1135	5.0150	−5.0073	5.3073	−2.0469	2.2362	−17.247	17.102	0.0590	−0.0611	0.6075	5.9169	0.4962
	15×15	0.1077	−0.1135	5.0150	−5.0072	5.3073	−2.0411	2.2308	−17.247	17.102	0.0590	−0.0611	0.6170	5.9178	0.4961
	3D solution	0.108	−0.114	5.015	−5.007	5.307	−2.043	2.232	−17.247	17.102	0.059	−0.061	0.617	5.917	0.496

[a] Values of the normal stress $\bar{\sigma}_{22}$correspond to the central layer.

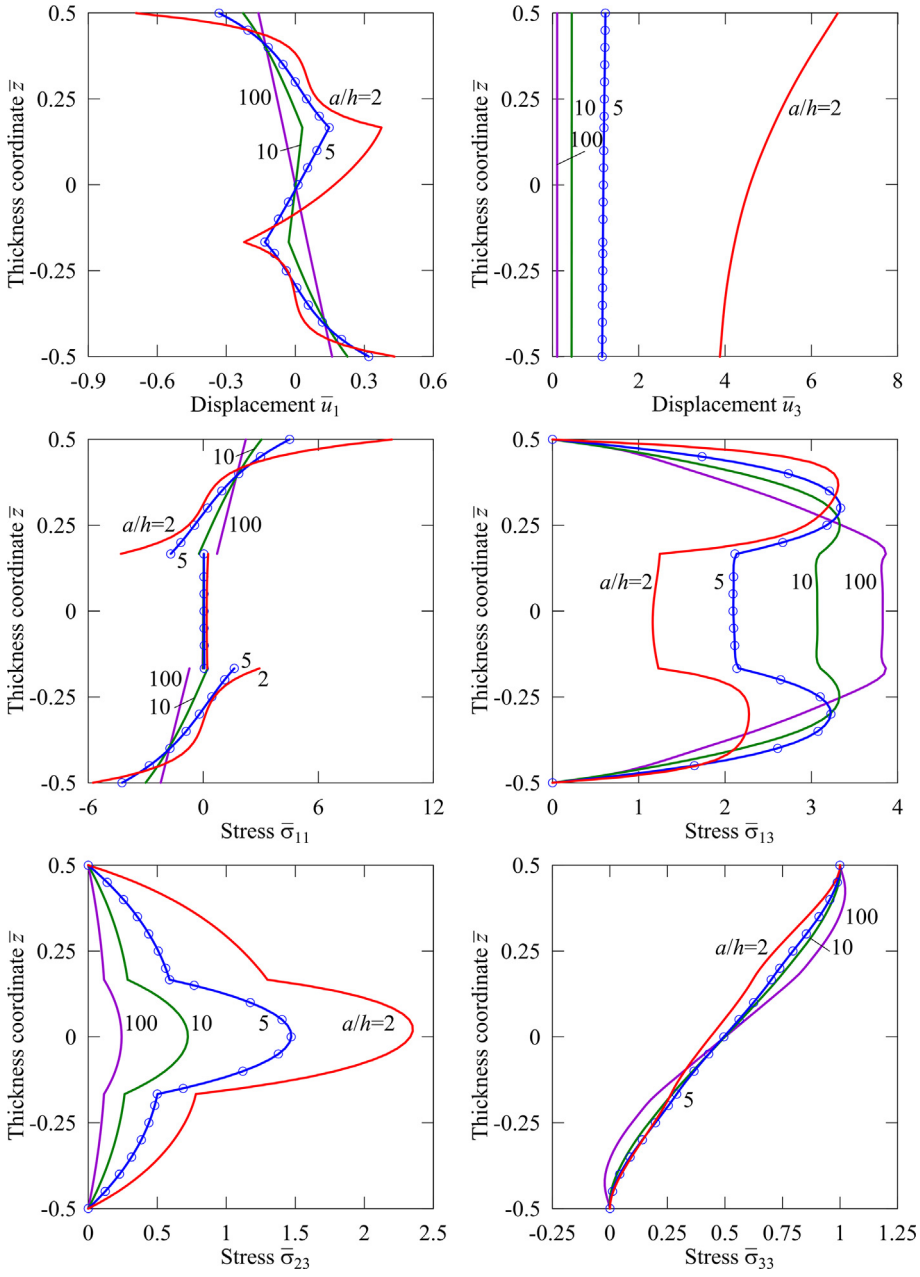

Fig. 4. Through-thickness distributions of displacements and stresses for the CSCS laminate under sinusoidal loading: SaS/EDQ formulation using nine SaS in each layer and 13×13 grid (solid lines) and Vel-Batra solution (○) [32].

Table 5
Results of the convergence study for the CCCC angle-ply laminates with stacking sequences $[-45/45/-45]$ (case 1) and $[-45/45/0]$ (case 2) with $b/a = 0.5$, $a/h = 5$ and nine SaS in each layer ($N_{SaS} = 27$).

Lamina	$N_1 \times N_2$	$\bar{u}_1(-0.5)$	$\bar{u}_1(0.5)$	$\bar{u}_2(-0.5)$	$\bar{u}_2(0.5)$	$\bar{u}_3(0)$	$\bar{\sigma}_{11}(-0.5)$	$\bar{\sigma}_{11}(0.5)$	$\bar{\sigma}_{22}(-0.5)$	$\bar{\sigma}_{22}(0.5)$	$\bar{\sigma}_{12}(-0.5)$	$\bar{\sigma}_{12}(0.5)$	$\bar{\sigma}_{13}(0)$	$\bar{\sigma}_{23}(0)$	$\bar{\sigma}_{33}(0)$
Case 1	7×7	0.1400	−0.1487	0.2033	−0.2245	1.5771	−0.8731	1.1294	−1.0126	1.2843	0.4585	−0.5661	0.6046	1.3032	0.4797
	9×9	0.1380	−0.1461	0.2029	−0.2238	1.5793	−0.9000	1.1620	−1.0451	1.3232	0.4482	−0.5548	0.6020	1.3037	0.4798
	11×11	0.1399	−0.1484	0.2040	−0.2250	1.5787	−0.8947	1.1576	−1.0409	1.3201	0.4557	−0.5614	0.5987	1.3001	0.4799
	13×13	0.1397	−0.1482	0.2040	−0.2250	1.5789	−0.8948	1.1565	−1.0404	1.3180	0.4513	−0.5564	0.5988	1.3005	0.4798
	SOLID45	0.1396	−0.1480	0.2037	−0.2247	1.5762	−0.8946	1.1567	−1.0403	1.3184	0.4520	−0.5578	0.5978	1.2992	0.4798
Case 2	7×7	0.1512	−0.1026	0.2244	−0.3311	1.7574	−1.0023	1.4508	−1.1583	0.4385	0.5530	−0.0577	0.7337	1.3626	0.5360
	9×9	0.1491	−0.1022	0.2243	−0.3286	1.7608	−1.0362	1.5092	−1.1966	0.4599	0.5392	−0.0574	0.7336	1.3644	0.5363
	11×11	0.1515	−0.1024	0.2254	−0.3298	1.7601	−1.0290	1.4978	−1.1910	0.4560	0.5464	−0.0577	0.7306	1.3607	0.5365
	13×13	0.1514	−0.1025	0.2255	−0.3304	1.7604	−1.0287	1.4964	−1.1902	0.4536	0.5419	−0.0576	0.7305	1.3611	0.5362
	SOLID45	0.1512	−0.1024	0.2252	−0.3299	1.7579	−1.0286	1.4957	−1.1902	0.4549	0.5427	−0.0575	0.7298	1.3598	0.5363

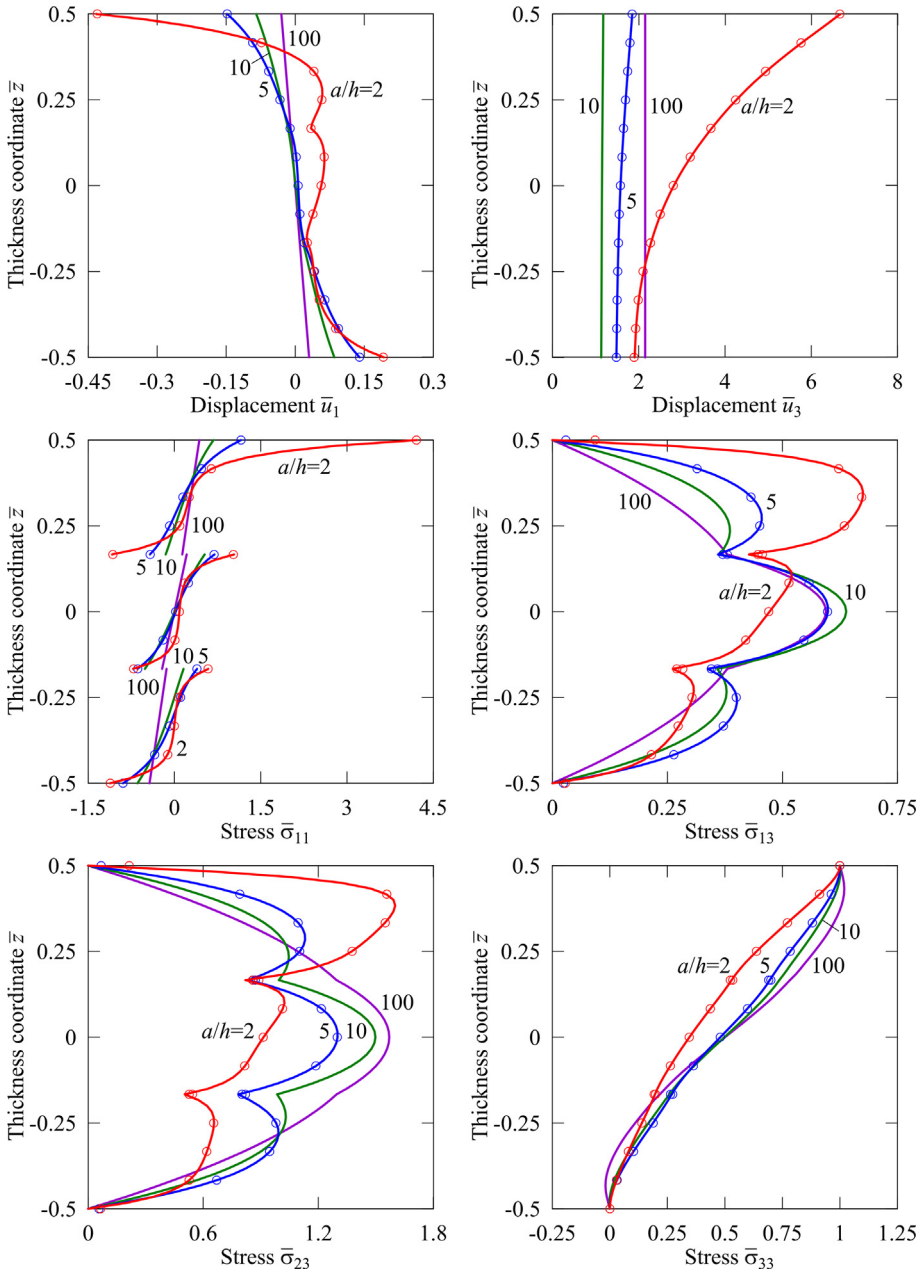

Fig. 5. Through-thickness distributions of displacements and stresses for the CCCC $[-45/45/-45]$ laminate with $b/a = 0.5$ under sinusoidal loading: SaS/EDQ formulation using nine SaS in each layer and 13×13 grid (solid lines) and SOLID45 element (○).

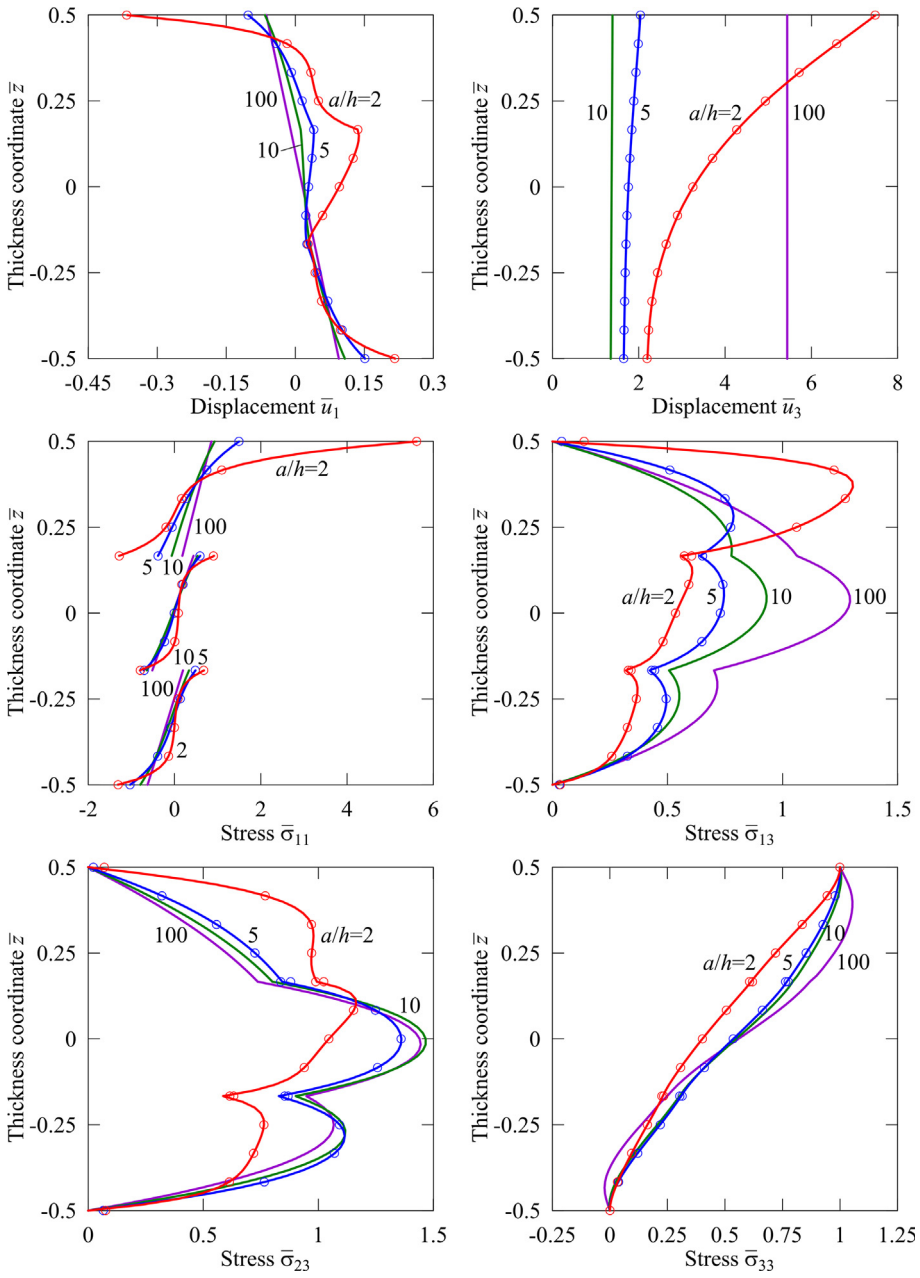

Fig. 6. Through-thickness distributions of displacements and stresses for the CCCC $[-45/45/0]$ laminate with $b/a = 0.5$ under sinusoidal loading: SaS/EDQ formulation using nine SaS in each layer and 13×13 grid (solid lines) and SOLID45 element (○).

SaS located at Chebyshev polynomial nodes within the layers and direct integration of the equilibrium equations of elasticity. The use of only Chebyshev polynomial nodes makes it possible to minimize uniformly the error due to Lagrange interpolation. Therefore, the developed strong SaS formulation allows obtaining the solutions for laminated composite plates with a prescribed accuracy, which asymptotically approach the exact solutions of elasticity as the number of SaS tends to infinity. To consider laminates with general boundary and loading conditions, the EDQ method is used, in which displacements, strains and stresses are interpolated in a rectangle using the Chebyshev-Gauss-Lobatto grid. This technique deals with only first-order derivatives in equilibrium equations [63]. Thus, the use of higher order derivatives is avoided that simplifies the implementation of the EDQ method and can be applied efficiently to high-precision calculations for the angle-ply laminates with arbitrary boundary conditions.

The future works will present the extension of the SaS/EDQ formulation to the three-dimensional analysis of laminated composite shells. The proposed technique is also convenient to develop the robust numerical algorithms for the laminated quadrilateral plates.

Declaration of Competing Interest

The authors declare that they have no known competing financial interests or personal relationships that could have appeared to influence the work reported in this paper.

Acknowledgement

This work was supported by the Russian Science Foundation (Grant No. 18-19-00092).

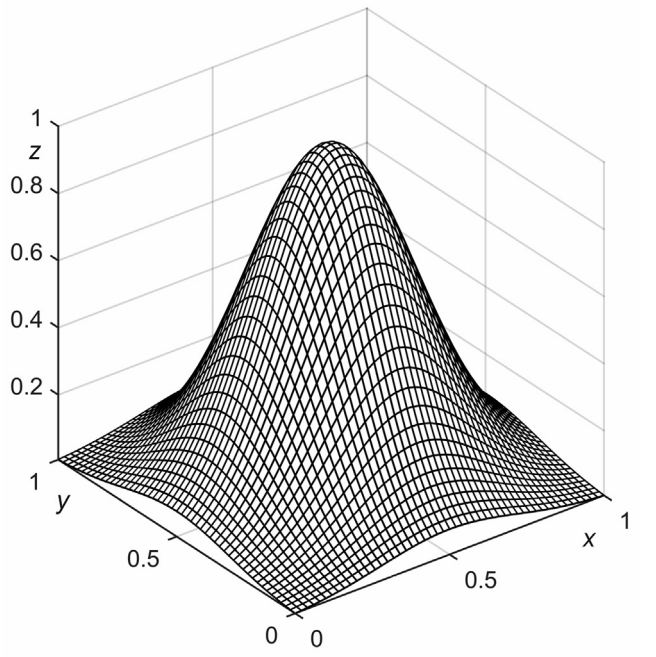

Fig. 7. Exponentially distributed load on the top surface.

Appendix A

The vectors $\mathbf{\Lambda}^{(n)i_n}_{ijn_1n_2}$ and $\mathbf{\Gamma}^{(n)i_n}_{in_1n_2}$ introduced in section 4 to define the SaS strains and boundary conditions at the grid points can be written in a closed form. The use of Eqs. (40), (41), (46) and (47) leads to the following expressions for the components of these vectors:

$$\left(\mathbf{\Lambda}^{(n)i_n}_{i1n_1n_2}\right)_{i+3(k_1-1)+3N_1(n_2-1)+3N_1N_2(\Delta_n+i_n-1)} = M_{k_1}(x_{n_1}),$$

$$\left(\mathbf{\Lambda}^{(n)i_n}_{i2n_1n_2}\right)_{i+3(n_1-1)+3N_1(k_2-1)+3N_1N_2(\Delta_n+i_n-1)} = M_{k_2}(y_{n_2}),$$

$$\left(\mathbf{\Lambda}^{(n)i_n}_{i3n_1n_2}\right)_{i+3(n_1-1)+3N_1(n_2-1)+3N_1N_2(\Delta_n+j_n-1)} = M^{(n)j_n}(z^{(n)i_n}),$$

$$\left(\mathbf{\Gamma}^{(n)i_n}_{in_1n_2}\right)_{i+3(n_1-1)+3N_1(n_2-1)+3N_1N_2(\Delta_n+i_n-1)} = 1,$$

$$\Delta_n = \sum_{\gamma=1}^{n-1} I_\gamma,$$

where the indices $i, j = 1, 2, 3$; $n = 1, 2, ..., N$; $i_n, j_n = 1, 2, ..., I_n$; $n_1,\ k_1 = 1, 2, ..., N_1$; $n_2,\ k_2 = 1, 2, ..., N_2$. The components of vectors not written out explicitly are equal to zero.

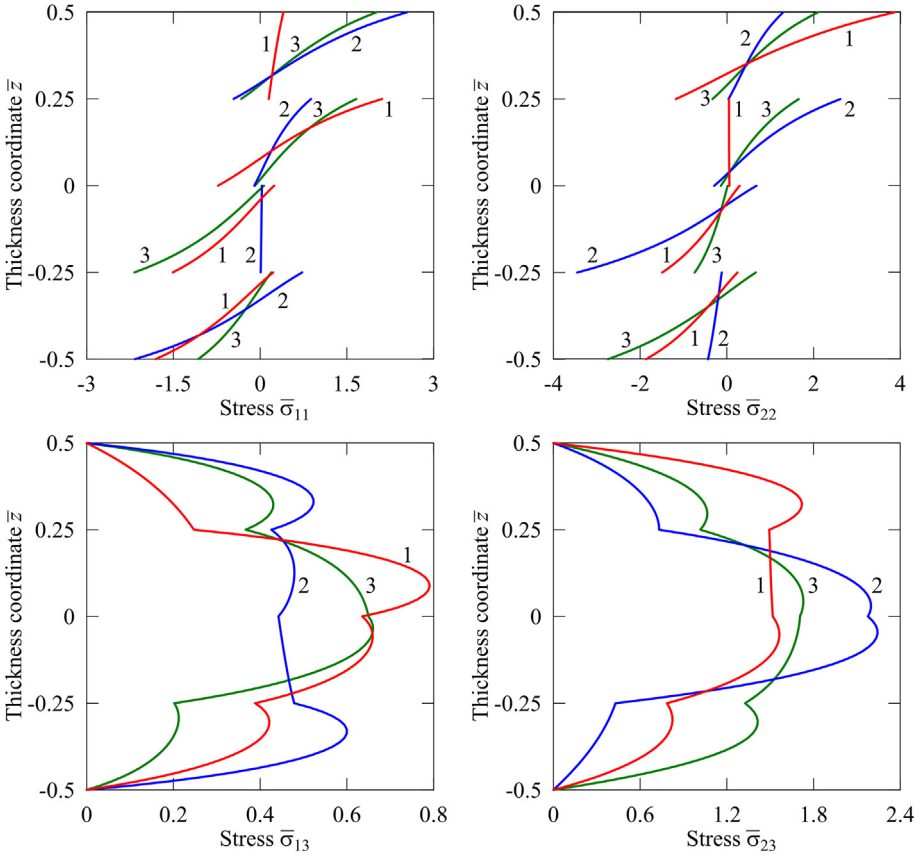

Fig. 8. Through-thickness distributions of stresses for the FCCC laminate with stacking sequences [45/ − 45/0/90] (case 1), [0/90/ − 60/30] (case 2) and [−60/30/45/ − 45/] (case 3) under exponential loading using nine SaS in each layer and 13 × 13 grid.

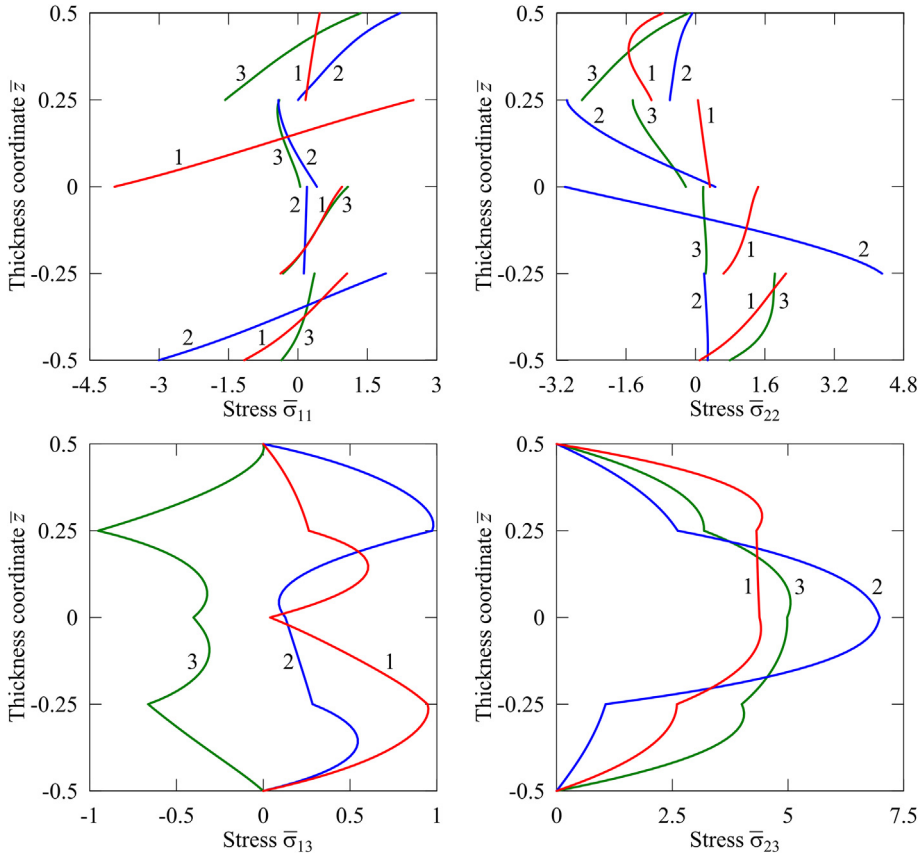

Fig. 9. Through-thickness distributions of stresses for the FCFF laminate with stacking sequences [45/ − 45/0/90] (case 1), [0/90/ − 60/30] (case 2) and [−60/30/45/ − 45] (case 3) under exponential loading using nine SaS in each layer and 13 × 13 grid.

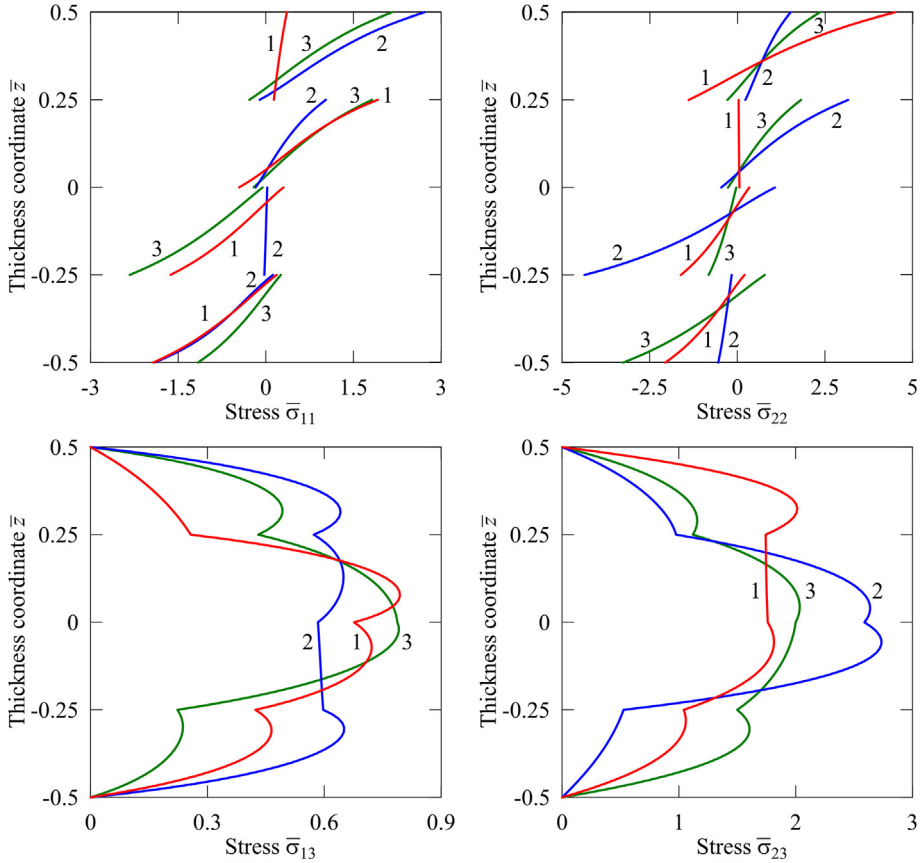

Fig. 10. Through-thickness distributions of stresses for the FCFC laminate with stacking sequences [45/ − 45/0/90] (case 1), [0/90/ − 60/30] (case 2) and [−60/30/45/ − 45/] (case 3) under exponential loading using nine SaS in each layer and 13 × 13 grid.

References

[1] Pagano NJ. Exact solutions for composite laminates in cylindrical bending. J Compos Mater 1969;3(3):398–411.
[2] Pagano NJ. Exact solutions for rectangular bidirectional composites and sandwich plates. J Compos Mater 1970;4(1):20–34.
[3] Brogan WL. Modern control theory. New Jersey: Prentice Hall; 1985.
[4] Frobenius G. Ueber die Integration der linearen Differentialgleichungen durch Reihen. J Reine Angew Math 1873;76:214–35.
[5] Gol'denveizer AN. Theory of thin elastic shells. New York: Pergamon Press; 1961.
[6] Kulikov GM, Plotnikova SV. Exact 3D stress analysis of laminated composite plates by sampling surfaces method. Compos Struct 2012;94(12):3654–63.
[7] Srinivas S, Rao Akella Kameswara, Joga Rao CV. Flexure of simply supported thick homogeneous and laminated rectangular plates. ZAMM 1969;49(8):449–58.
[8] Srinivas S, Rao AK. Bending, vibration and buckling of simply supported thick orthotropic rectangular plates and laminates. Int J Solids Struct 1970;6 (11):1463–81.
[9] Srinivas S, Joga Rao CV, Rao AK. An exact analysis for vibration of simply-supported homogeneous and laminated thick rectangular plates. J Sound Vib 1970;12(2):187–99.
[10] Noor AK, Burton WS. Three-dimensional solutions for antisymmetrically laminated anisotropic plates. J Appl Mech 1990;57:182–8.
[11] Tungikar VB, Rao Koganti M. Three dimensional exact solution of thermal stresses in rectangular composite laminate. Compos Struct 1994;27(4):419–30.
[12] Bhaskar K, Varadan TK, Ali JSM. Thermoelastic solutions for orthotropic and anisotropic composite laminates. Compos Part B 1996;27(5):415–20.
[13] Batra RC, Aimmanee S. Missing frequencies in previous exact solutions of free vibrations of simply supported rectangular plates. J Sound Vib 2003;265 (4):887–96.
[14] Iyengar KTSR, Chandrashekhara K, Sebastian VK. On the analysis of thick rectangular plates. Ingenieur-Archiv 1974;43(5):317–30.
[15] Sundara Raja Iyengar KT, Pandya SK. Analysis of orthotropic rectangular thick plates. Fiber Sci Technol 1983;18(1):19–36.
[16] Jiarang Fan, Jianqiao Ye. An exact solution for the statics and dynamics of laminated thick plates with orthotropic layers. Int J Solids Struct 1990;26(5-6):655–62.
[17] Loredo A. Exact 3D solution for static and damped harmonic response of simply supported general laminates. Compos Struct 2014;108:625–34.
[18] Vel Senthil S, Batra RC. Exact solution for thermoelastic deformations of functionally graded thick rectangular plates. AIAA J 2002;40(7):1421–33.
[19] Vel Senthil S, Batra RC. Three-dimensional analysis of transient thermal stresses in functionally graded plates. Int J Solids Struct 2003;40(25):7181–96.
[20] Vel Senthil S, Batra RC. Three-dimensional exact solution for the vibration of functionally graded rectangular plates. J Sound Vib 2004;272(3-5):703–30.
[21] Jiann-Quo Tarn, Yung-Ming Wang. An asymptotic theory for dynamic response of anisotropic inhomogeneous and laminated plates. Int J Solids Struct 1994;31 (2):231–46.
[22] Yung-Ming Wang, Jiann-Quo Tarn. A three-dimensional analysis of anisotropic inhomogeneous and laminated plates. Int J Solids Struct 1994;31(4):497–515.
[23] Tarn Jiann-Quo. An asymptotic variational formulation for dynamic analysis of multilayered anisotropic plates. Comput Methods Appl Mech Eng 1996;130(3-4):337–53.
[24] Reddy JN, Cheng ZQ. Three-dimensional thermomechanical deformations of functionally graded rectangular plates. Eur J Mech A/Solids 2001;20:841–55.
[25] Reddy JN, Cheng Zhen-Qiang. Frequency of functionally graded plates with three dimensional asymptotic approach. J Eng Mech 2003;129(8):896–900.
[26] Kulikov GM, Plotnikova SV. Strong sampling surfaces formulation for laminated composite plates. Compos Struct 2017;172:73–82.
[27] Kulikov GM, Plotnikova SV, Kulikov MG. Strong SaS formulation for free and forced vibrations of laminated composite plates. Compos Struct 2017;180:286–97.
[28] Kulikov GM, Plotnikova SV. Strong sampling surfaces formulation for layered shells. Int J Solids Struct 2017;121:75–85.
[29] Kulikov GM, Plotnikova SV, Kulikov MG. Three-dimensional vibration analysis of simply supported laminated cylindrical shells and panels by a strong SaS formulation. ZAMM 2019;99(1):e201800100. https://doi.org/10.1002/zamm.v99.110.1002/zamm.201800100.
[30] Srinivas S, Rao AK. Flexure of thick rectangular plates. J Appl Mech 1973;39:298–9.
[31] Hutchinson JR, Zillimer SD. Vibration of a free rectangular parallelepiped. J Appl Mech 1983;50:123–30.
[32] Vel Senthil S, Batra RC. Analytical solution for rectangular thick laminated plates subjected to arbitrary boundary conditions. AIAA J 1999;37(11):1464–73.
[33] Kumari Poonam, Kapuria Santosh, Rajapakse RKND. Three-dimensional extended Kantorovich solution for Levy-type rectangular laminated plates with edge effects. Comp Struct 2014;107:167–76.
[34] Ye JQ. A three-dimensional free vibration analysis of cross-ply laminated rectangular plates with clamped edges. Comput Methods Appl Mech Eng 1997;140(3-4):383–92.
[35] Leissa Arthur, Zhang Zhong-ding. On the three-dimensional vibrations of the cantilevered rectangular parallelepiped. J Acoust Soc Am 1983;73(6):2013–21.
[36] Liew KM, Hung KC, Lim MK. A continuum three-dimensional vibration analysis of thick rectangular plates. Int J Solids Struct 1993;30(24):3357–79.
[37] Messina Arcangelo, Rollo Giosuè. Three-dimensional free vibration analysis of cross-ply laminated rectangular plates with free edges through a displacement-based approach. Math Mech Solids 2010;15(5):539–56.
[38] Messina Arcangelo. Influence of the edge-boundary conditions on three-dimensional free vibrations of isotropic and cross-ply multilayered rectangular plates. Compos Struct 2011;93(8):2135–51.
[39] Ye Tiangui, Jin Guoyong. Elasticity solution for vibration of generally laminated beams by a modified Fourier expansion-based sampling surface method. Comput Struct 2016;167:115–30.
[40] Ye Tiangui, Jin Guoyong, Su Zhu. Three-dimensional vibration analysis of sandwich and multilayered plates with general ply stacking sequences by a spectral-sampling surface method. Compos Struct 2017;176:1124–42.
[41] Kulikov GM. Refined global approximation theory of multilayered plates and shells. J Eng Mech 2001;127(2):119–25.
[42] Kulikov GM, Plotnikova SV. On the use of a new concept of sampling surfaces in a shell theory. Adv Struct Mater 2011;15:715–26.
[43] Kulikov GM, Plotnikova SV, Mamontov AA. Sampling surfaces formulation for thermoelastic analysis of laminated functionally graded shells. Meccanica 2016;51 (8):1913–29.
[44] Kulikov GM, Plotnikova SV, Kulikov MG, Monastyrev PV. Three-dimensional vibration analysis of layered and functionally graded plates through sampling surfaces formulation. Compos Struct 2016;152:349–61.
[45] Kulikov GM, Bohlooly Mehdi, Plotnikova SV, Kouchakzadeh MA, Glebov AO. Nonlinear displacement-based and hybrid-mixed quadrilaterals for three-dimensional stress analysis through sampling surfaces formulation. Thin-Walled Struct 2020;155:106918. https://doi.org/10.1016/j.tws.2020.106918.
[46] Kulikov GM, Plotnikova RS. Solution of three-dimensional problems for thick elastic shells by the method of reference surfaces. Mech Solids 2014;49(4):403–12.
[47] Bellman Richard, Casti John. Differential quadrature and long-term integration. J Math Anal Appl 1971;34(2):235–8.
[48] Bellman Richard, Kashef BG, Casti J. Differential quadrature: A technique for the rapid solution of nonlinear partial differential equations. J Comput Phys 1972;10 (1):40–52.
[49] Bert Charles W, Jang Sung K, Striz Alfred G. Two new approximate methods for analyzing free vibration of structural components. AIAA J 1988;26(5):612–8.
[50] Bert Charles W, Xinwei Wang, Striz Alfred G. Differential quadrature for static and free vibration analyses of anisotropic plates. Int J Solids Struct 1993;30 (13):1737–44.
[51] Shu Chang, Richards Bryan E. Application of generalized differential quadrature to solve two-dimensional incompressible Navier-Stokes equations. Int J Numer Methods Fluids 1992;15(7):791–8.
[52] Shu Chang, editor. Differential Quadrature and Its Application in Engineering. London: Springer London; 2000.
[53] Liew KM, Teo TM. Modeling via differential quadrature method: Three-dimensional solutions for rectangular plates. Comput Methods Appl Mech Eng 1998;159(3-4):369–81.
[54] Teo TM, Liew KM. A differential quadrature procedure for three-dimensional buckling analysis of rectangular plates. Int J Solids Struct 1999;36(8):1149–68.
[55] Teo TM, Liew KM. Three-dimensional elasticity solutions to some orthotropic plate problems. Int J Solids Struct 1999;36(34):5301–26.
[56] Bert CW, Malik M. Differential quadrature method in computational mechanics. Appl Mech Rev 1996;49:1–28.
[57] Tornabene F, Fantuzzi N, Ubertini F, Viola E. Strong formulation finite element method based on differential quadrature: A survey. Appl Mech Rev 2015;67:020801.
[58] Kulikov Gennady M. Application of strong SaS formulation and enhanced DQ method to 3D stress analysis of rectangular plates. Eur J Mech A/Solids 2020;79:103861. https://doi.org/10.1016/j.euromechsol.2019.103861.
[59] Davis Timothy A. A column pre-ordering strategy for the unsymmetric-pattern multifrontal method. ACM Trans Math Software 2004;30(2):165–95.
[60] Davis Timothy A. Algorithm 832: UMFPACK V4.3 – an unsymmetric-pattern multifrontal method. ACM Trans Math Software 2004;30(2):196–9.
[61] Davis Timothy A, Duff Iain S. An unsymmetric-pattern multifrontal method for sparse LU factorization. SIAM J Matrix Anal Appl 1997;18(1):140–58.
[62] ANSYS 2019 R2 Release. Canonsburg, PA: ANSYS Inc; 2019.
[63] Kulikov GM, Kulikov MG. High-precision stress calculations for composite cylindrical shells with general boundary conditions using strong SaS formulation and extended DQ method. Mech Adv Mater Struct 2021. https://doi.org/10.1080/15376494.2021.1896058. In press.